1   **Title:** State-Unspecific Modes of Whole-Brain Functional Connectivity Predict Intelligence

2   and Life Outcomes

3

4   **Authors and author addresses:**

5   Yu Takagi[1,2,3*], Jun-ichiro Hirayama[4,1], Saori C Tanaka[1*]

6   [1] ATR Brain Information Communication Research Laboratory Group, Kyoto 619-0288,

7   Japan

8   [2] Graduate School of Information Science, Nara Institute of Science and Technology, Nara

9   630-0192, Japan.

10   [3] Japan Society for the Promotion of Science, Tokyo 102-0083, Japan

11   [4] RIKEN Center for Advanced Intelligence Project, Tokyo 103-0027, Japan.

12   ***Corresponding author**: yu.takagi@atr.jp (Yu Takagi), xsaori@atr.jp (Saori C. Tanaka)

13   **Conflict of Interest**: The authors declare no competing financial interests.

14

15 **Abstract**

16 Recent functional magnetic resonance imaging (fMRI) studies have increasingly revealed

17 potential neural substrates of individual differences in diverse types of brain function and

18 dysfunction. Although most previous studies have been inherently limited to state-specific

19 characterizations of related brain networks and their functions, several recent studies have

20 examined the potential state-unspecific nature of functional brain networks, such as their

21 global similarities across different experimental conditions (i.e., states) including both task

22 and rest. However, no previous studies have carried out direct, systematic characterizations

23 of state-unspecific brain networks, or their functional implications. Here, we quantitatively

24 identified several modes of state-unspecific individual variation in whole-brain functional

25 connectivity patterns, called "Common Neural Modes (CNMs)", from a large fMRI dataset

26 including eight task/rest states, obtained from the Human Connectome Project. Furthermore,

27 we tested how CNMs account for variability in individual behavioral measures. The results

28 revealed that three CNMs were robustly extracted under various different preprocessing

29 conditions. Each of these CNMs was significantly correlated with different aspects of

30 behavioral measures of both fluid and crystalized intelligence. The three CNMs were also

31 able to predict several life outcomes, such as income and life satisfaction, achieving the

32 highest performance when combined with behavioral intelligence measures as inputs. Our

33 findings highlight the importance of state-unspecific brain networks to characterize

34 fundamental individual variation.

35

38

Introduction

An increasing number of cognitive neuroscience studies have revealed the neural substrates of individual difference using functional magnetic resonance imaging (fMRI) (Dubois and Adolphs, 2016) by investigating coordinated activation (co-activation) patterns of the whole brain. The degree of co-activation between different brain regions of interest (ROIs), often referred to as functional connectivity (FC), is typically measured by the correlation between the blood-oxygen-level-dependent (BOLD) signals averaged within each ROI. A set of brain regions that cooperates under some experimental conditions is typically called a "network", as represented by the default mode network (DMN) (Raichle, 2015). A wide variety of individual differences in our cognition and behavior have been associated with the characteristics of FC patterns and networks in the brain, including cognitive abilities (Finn et al., 2015; Smith et al., 2015), sustained attention ability (Rosenberg et al., 2016), emotional sensitivity (Modi et al., 2015; Takagi et al., 2018) and psychiatric disorders (Fox and Greicius, 2010; Takagi et al., 2017).

These previous studies have investigated the relationship between individual differences and brain networks while a person is experiencing a specific state. In particular, recent research has intensively focused on the resting state, as it potentially reflects many types of individual differences and can be measured easily (Dubois and Adolphs, 2016). The present study is directly inspired by Smith et al. (2015), who revealed, in a data-driven manner, that a small number of linear factors underlying individuals' whole-brain resting-state FC patterns ("neural modes") can explain diverse ranges of individual differences simultaneously (Smith et al., 2015). However, despite their apparent connections with behavior, the brain networks and neural modes examined in these previous studies, as well as their relations to individual differences, are inherently state-specific; thus, it is unclear whether these findings generalize across states, indicating basic traits of individuals. Geerligs et al. (2015) demonstrated that the relationship between individual differences and FC patterns may substantially change across different states, including both rest and task (Geerligs et al., 2015).

3

69   A small number of recent studies have suggested the existence of more fundamental, "state-
70   unspecific" brain networks which characterize individuals in a similar manner across
71   different states (Cole et al., 2014; Finn et al., 2015; Tavor et al., 2016). Specifically, Cole et
72   al. (2014) found that average FC patterns of a number of subjects exhibit a high degree of
73   global similarity among different states, including rest. Finn et al. (2015) reported that FC
74   patterns of each individual were also globally similar, across various task and rest states.
75   Furthermore, Tavor et al. (2016) revealed that an individual's brain activity during a task state
76   can be predicted from their resting-state FC patterns. These findings clearly suggest a
77   potential state-unspecific aspect of brain networks. Unfortunately, however, no previous
78   studies have explicitly identified these state-unspecific brain networks, or quantitatively
79   investigated their relationship to individual differences in behavior.

80

81   In the present study, we conducted, for the first time, a quantitative characterization of state-
82   unspecific brain networks and investigated its connection with inter-individual variability in
83   behavior. Our approach combined the large-scale database of the Human Connectome Project
84   with a sophisticated machine learning technique. Specifically, we applied multiset canonical
85   correlation analysis (M-CCA) to the FC matrices obtained from eight states, including the
86   resting state (Kettenring, 1971; Vía et al., 2007). The obtained components uniquely
87   characterize individuals' FC patterns that are common across different states, which we refer
88   to as "Common Neural Modes (CNMs)". We demonstrated that several CNMs could be
89   robustly extracted from whole-brain FC patterns. These CNMs were then found to be
90   selectively correlated with behavioral intelligence measures. In addition, we demonstrated
91   that CNMs could predict several types of life outcomes, complementing conventional
92   behavioral measures of intelligence.

Materials and methods

Subjects

We used a public fMRI dataset available from the Human Connectome Project (HCP) 500 Subject Release (Van Essen et al., 2012) (http://humanconnectome.org/data). We excluded 1) subjects who did not have all eight fMRI datasets (corresponding to seven task states and one resting state) or who were not given all 44 behavioral measures (subdivided into 12 categories of cognition), and 2) subjects who exhibited substantial movement during fMRI data acquisition (see fMRI preprocessing). After this screening process, 406 subjects were included in the final analysis. All subjects were healthy adults (ages 22–36 years, 238 females).

MRI parameters

The fMRI data were acquired using a protocol with advanced multiband sequences. Whole-brain echo-planar scans were acquired with a 32-channel head coil on a modified 3T Siemens Skyra with repetition time = 720 ms, echo time = 33.1 ms, flip angle = 52°, bandwidth 2,290 Hz/Px, in-plane field of view = 208 ×180 mm, 72 slices, 2.0 mm isotropic voxels, with a multiband acceleration factor of 8 (Uğurbil et al., 2013). Data were collected over 2 days. On each day, 28 min of rest (eyes open with fixation) fMRI data across two runs were collected (two runs, 56 min in total, per day), followed by 30 min of task-fMRI data collection (60 min in total, per day). Each of the seven task-fMRI was completed over two consecutive fMRI runs. Three task-fMRI (working memory, reward learning, and motor responses) data were collected on the first day. The other four task-fMRI (emotion perception, language processing, relational reasoning, and social cognition) data were collected on the second day. More details about the fMRI collection method were described in previous studies (Barch et al., 2013; Smith et al., 2013).

Task paradigms

The seven task-fMRI paradigms were selected to activate different neural circuitry that supports broad cognitive functions, and included emotion perception, reward learning,

5

123   language processing, motor responses, relational reasoning, social cognition, and working

124   memory (Barch et al., 2013; Cole et al., 2016). Briefly, the emotion task involved matching

125   fearful or angry faces to a target face. The reward learning task involved a gambling task

126   involving monetary rewards and losses. The language task involved auditory stimuli

127   consisting of narrative stories and math problems, along with questions to be answered

128   regarding the prior auditory stimuli. The motor task involved movement of the hands, tongue

129   and feet. The relational reasoning task involved higher-order cognitive reasoning regarding

130   relations among features of presented shape stimuli. The social cognition (theory of mind)

131   task used short video clips of moving shapes that interacted in some way or moved randomly,

132   with subjects making decisions about whether the shapes had social interactions. The

133   working memory task involved the conventional visual 2-back and 0-back tasks.

134

135   **fMRI preprocessing**

136   Fig. 1 shows a schematic diagram of our analysis. The datasets were originally preprocessed

137   through the HCP minimal preprocessing pipeline (Glasser et al., 2013). This pipeline includes

138   artefact removal, motion correction and registration to standard space. T1 images were

139   segmented into three tissue classes in Montreal Neurological Institute (MNI) space using

140   Statistical Parametric Mapping 8 (SPM8: Wellcome Department of Cognitive Neurology,

141   http:/ /www.fil.ion.ucl.ac.uk/spm/software/) in MATLAB (The MathWorks, Inc., Natick,

142   MA). First, for each subject, the framewise displacement (FD) at each scan was calculated

143   by summing up all six head motion parameters. The "scrubbing" procedure (Power et al.,

144   2012) then identified scans that exhibited excessive head motion based on FD volumes.

145   Specifically, a scan was flagged if the FD exceeded 0.5 mm. The flagged scan, the preceding

146   scan, and the two subsequent scans, were excluded from the correlation analysis below.

147   Subjects were excluded from the subsequent analyses if less than 50% of the scans remained

148   after this procedure for any of the eight fMRI data sets. Then, for each subject, pair-wise,

149   interregional FC was evaluated among 268 ROIs covering the entire brain (Finn et al., 2015)

150   (atlas can be downloaded from https://www.nitrc.org/frs/?group_id=51). The representative

151   time course of each region was extracted by averaging the BOLD time courses of the voxels

152   within that region. Each ROI time course was linearly regressed on the temporal fluctuations

6

153   of both the white matter and the cerebrospinal fluid as well as the six head motion parameters,

154   whose effects were then subtracted from the original time course. The fluctuation of each

155   tissue class was the average time course of the voxels within the corresponding mask. After

156   within-run linear trend removal, for each subject, we calculated an FC matrix consisting of

157   all the pairwise FCs between the 268 ROIs, based only on the remaining scans after the

158   scrubbing step above. As the FC matrices are symmetric, values on only the strictly lower

159   part were kept, resulting in 35,778 (= 268 × 267 / 2) unique entries (FC values) (Fig. 1a). For

160   all task and resting state fMRI data, FC matrices were calculated using the same procedure.

161   Note that an FC matrix was obtained for every run, and those of multiple runs were averaged

162   in each of the eight task or resting-state conditions.

163

164
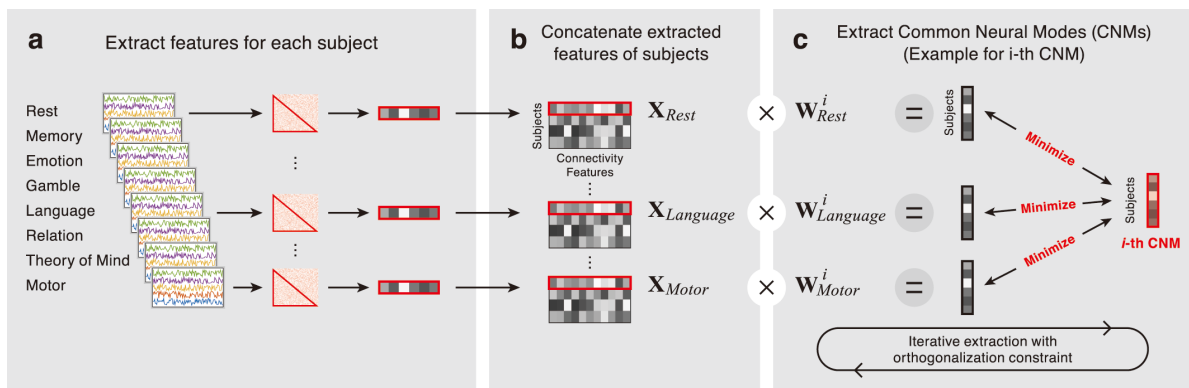
Figure 1. Schematic diagram of the analyses. (1) For each subject, feature vectors from
the eight states were extracted. (2) Within each state, data for all subjects were
concatenated to obtain input data matrices. (3) Common Neural Modes (CNMs) were
calculated by minimizing the difference between weighted input matrices and CNMs.
CNMs were iteratively calculated with the orthogonalization constraint.

170

171

Identifying CNMs

173   We identified common neural modes (CNMs) of individuals as FC patterns that robustly

174   characterized individuals irrespective of state. Specifically, we used M-CCA (Kettenring,

175   1971), which extends canonical correlation analysis (CCA) (Hotelling, 1936) to more than

176 two datasets. Both methods identify canonical variates that summarize each dataset by linear

177 transformations. In contrast, conventional CCA maximizes correlations between a pair of

178 canonical variates, M-CCA maximizes a scalar objective function that summarizes all

179 pairwise correlations among M (> 2) canonical variates. M-CCA reduces to CCA when the

180 number of datasets M is two. Several variants of M-CCA have been proposed, depending on

181 how it summarizes the pairwise correlations into a single objective function (Kettenring,

182 1971). We chose the MAXVAR approach because it explicitly introduces common latent

183 factors across different datasets (Vía et al., 2007), which can be naturally interpreted as

184 CNMs.

185 Suppose that we are given M data matrices $\mathbf{X}_k \in \mathbb{R}^{N \times m_k}$, $k = 1,...,M$ (Fig. 1b), where N

186 denotes the sample size and m_k denotes the dimensionality of the k-th data space. Each

187 column is assumed to have zero sample mean, without loss of generality. The MAXVAR

188 approach can then be stated as the problem of finding M weight vectors $\mathbf{w}_k$ ($k = 1,...,M$), each

189 for one of the M datasets, so that the errors between the corresponding canonical factors $\mathbf{X}_k\mathbf{w}_k$

190 and their grand average $\mathbf{z} \in \mathbb{R}^{N \times 1}$ is minimized. The cost function to be minimized is

191 formally given as

192
$$J = \min \sum_{k=1}^{M} \|\mathbf{z} - \mathbf{X}_k\mathbf{w}_k\|^2.$$

193 where the minimization is performed with respect to both $\mathbf{w}_k$ and $\mathbf{z}$. To avoid trivial solutions,

194 $\mathbf{w}_k$ and $\mathbf{z}_k$ are constrained to have unit Euclidean norms, and to be mutually orthogonal. The

195 solution is given by solving a generalized eigenvalue problem. See Via et al. (2005) for more

196 detailed information about this procedure. Solving this problem gives a set of M vectors $\mathbf{w}_k$,

197 and CNMs are defined as the average of $\mathbf{X}_k\mathbf{w}_k$ for k = 1,…,M (Fig. 1c).

198 To reduce redundancy among FCs, the dimensionalities of the data matrices were reduced in

199 advance using principal components analysis (PCA). The numbers of principal components

200 were varied between 10, 50 and 100 for calculating CNMs, and the numbers of CNMs were

201 also varied between 10, 50 and 100, respectively. The significance of the pairwise canonical

202 correlations was investigated using a permutation test for individual CNMs. We first shuffled

203 subject labels of all $\mathbf{X}_k$, then conducted M-CCA. We ran these analyses 1,000 times and

8

204   obtained 1,000 instances of estimated $\mathbf{w}_k$. We then took the average of the absolute correlation

205   coefficients between all pairs among $\mathbf{X}_k\mathbf{w}_k$ for each random dataset. Finally, we calculated

206   the statistical significance by comparing the true averaged value of the correlation coefficient

207   with those obtained from shuffled datasets.

208

209   **Relationship between CNMs and cognitive measures**

210   To analyze how CNMs were associated with individual differences in behavior, we calculated

211   Pearson's correlations between the CNMs and cognitive measures obtained using HCP with

212   various behavioral test batteries. The targets of those cognitive measures include, for example,

213   episodic memory, executive function, self-regulation, language and fluid intelligence. The

214   original set of measures were available from the HCP database website. When both age-

215   adjusted and age-unadjusted versions existed for the same index, we excluded the age-

216   unadjusted version.

217   To reduce the risk of overfitting, we conducted all analyses in a fully cross-validated manner

218   (Barch and Yarkoni, 2013). Specifically, we first split all the subjects into 10 disjointed

219   subsets of subjects. The model for calculating CNMs was then obtained based on all but one

220   set of subjects (training set) and the model was then tested on the one withheld set of subjects

221   (test set). We repeated this procedure 10 times (10-fold cross validation).

222

223   **Prediction of life outcomes using CNMs**

224   The preceding analysis suggested that CNMs correlated with representative intelligence

225   measures obtained by the behavioral test batteries. Thus we further investigated whether the

226   CNMs may account for individual differences in the subjects' life outcomes, which have been

227   considered to be predicted by intelligence measures in the field of educational psychology

228   (Cattell, 1963; Colom et al., 2010; Gottfredson, 1997). As a measure of life outcomes, we

229   chose three measures: income, life satisfaction and year of education. We conducted the

230   analysis using nested 10-fold cross validation. We first split all subjects into 10 sets of

231   subjects, and identified CNMs based on the training set, as with the previous analysis. We

232   then constructed a prediction model using 5-fold cross validation among the training set. We

233   used the L1-regularized linear regression model for each iteration. The hyper-parameter λ

9

234   (the regularization coefficient) was tuned by choosing the best value from $\lambda \in$

235   $\{0.0001, 0.001, 0.01, 0.1\}$ based on this inner 5-fold cross validation. We finally applied the

236   models for calculating CNMs and life outcomes to the test set. Performance was evaluated

237   by performing Pearson's correlation between predicted and actual life outcomes across whole

238   subjects.

239

240   **Effects of the number of states used to identify CNMs**

241   We investigated the effects of the number of states used to identify CNMs on prediction

242   accuracy. Specifically, we conducted the same prediction analyses as above, but here we used

243   a smaller number of states for constructing the CNMs. We varied the number of states for

244   constructing the CNMs from 2 to 8. We calculated all possible combinations for each case.

245   For example, we calculated 28 CNMs $(= \binom{8}{2})$, then constructed prediction models for all

246   CNMs, when we estimated the prediction accuracy of two states.

247

248   **Interpretation of CNMs**

249   To facilitate the characterization of the biological substrates of the CNMs, we summarized

250   the FC patterns that were correlated with first, second and third CNMs. We focused on these

251   three CNMs because they had been robustly extracted by M-CCA. First, we averaged every

252   FC value over all eight states. We then calculated Pearson's correlation coefficients between

253   three CNMs and each averaged FC. The 268 ROIs were then grouped into eight

254   representative macroscale networks (e.g., DMN) defined functionally in a previous study

255   (Finn et al., 2015). We then examined the number of FCs between each pair of regions in

256   each network. Finally, we visualized the relative numbers of FCs in each of the two networks

257   as the thickness of the connection lines (see Fig. 5). To aid interpretation, we visualized 200

258   FCs among all 38,578 FCs that were the most strongly correlated with the CNMs.

259

10

260 **Results**

261

262 **Characterization of CNMs**

263 We first determined the number of CNMs that exhibited significant pairwise canonical

264 correlations among eight states. For any choices of the preprocessing PCA dimensions (i.e.,

265 10, 50, and 100), first, second and third CNMs (namely CNM1, CNM2 and CNM3) exhibited

266 significant overall correlations between states (where all the pairwise correlations were

267 averaged) ($P < 0.001$ for all CNMs; 1,000 times permutation test); the other CNMs did not

268 ($P > 0.05$; 1,000 times permutation test). The M-CCA results were highly consistent under

269 different choices of PCA dimensions (see Supplementary Notes). We therefore focused on

270 the top three CNMs, obtained by M-CCA on 10 PCs of FC vectors.

271 We then investigated which cognitive measures correlated with each of the three CNMs. Figs.

272 2a, 2b and 2c show the distributions of the correlation coefficients between cognitive

273 measures and CNM1, CNM2 and CNM3, respectively. Table 1 shows representative

274 behavioral indices with significantly higher correlation coefficients than the chance level.

275 CNM1 was selectively correlated with fluid intelligence, which is a representative

276 component of general intelligence having a broad effect on our daily life and future success

277 (Cattell, 1963; Colom et al., 2010; Gottfredson, 1997). CNM2 correlated with various

278 language related scores (reading recognition and vocabulary comprehension) and self-

279 regulation (delay discounting). It is noteworthy that language related scores are related to

280 crystalized intelligence, a central component of general intelligence along with fluid

281 intelligence (Cattell, 1963; Gottfredson, 1997). Finally, CNM3 was correlated with both fluid

282 intelligence and language-related scores. Note that we confirmed that the correlations

283 described above were not simply the consequence of PCA, which maximizes the variability

284 between individuals in each state (see Supplementary Notes).

285
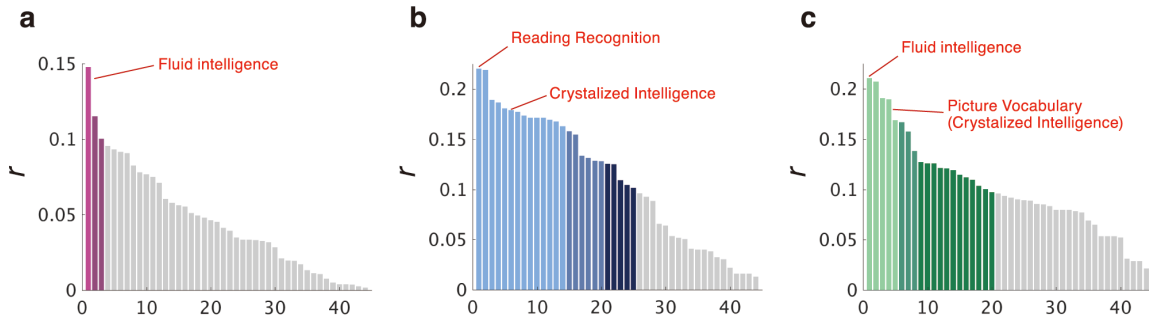
Figure 2. Absolute correlation coefficients (r) between each cognitive measure and the CNMs. Absolute correlation coefficients (r) between 44 cognitive measures and (a) CNM1, (b) CNM2 and (c) CNM3, respectively. The bar with light, medium, dark colored and grey indicated different levels of significance (P < 0.001, P < 0.01, P < 0.05 and P ≥ 0.05, respectively).

	CNM1		CNM2		CNM3	
	Name	**R**	**Name**	**R**	**Name**	**R**
	Penn Progressive Matrices: Number of Correct Responses	0.148	NIH Toolbox Oral Reading Recognition Test: Age-Adjusted Scale Score	0.221	Penn Progressive Matrices: Number of Correct Responses	0.211
	Penn Progressive Matrices: Total Skipped Items	0.115	Delay Discounting: Subjective Value for $200 at 1 year	0.219	Penn Progressive Matrices: Total Skipped Items	0.207
	Penn Emotion Recognition Test: Number of Correct Happy Identifications	0.100	Delay Discounting: Area Under the Curve for Discounting of $40,000	0.189	Variable Short Penn Line Orientation: Total Positions Off for All Trials	0.191

12

	Delay Discounting: Subjective Value for $40K at 5 years	0.187	NIH Toolbox Picture Vocabulary Test: Age-Adjusted Scale Score	0.189
	Delay Discounting: Subjective Value for $200 at 6 months	0.181	Delay Discounting: Subjective Value for $40K at 1 year	0.169
	NIH Toolbox Picture Vocabulary Test: Age-Adjusted Scale Score	0.179	Variable Short Penn Line Orientation: Total Number Correct	0.167
	Delay Discounting: Area Under the Curve for Discounting of $200	0.178	Penn Emotion Recognition Test: Number of Correct Responses	0.157
	Delay Discounting: Subjective Value for $200 at 3 years	0.174	Penn Emotion Recognition Test: Number of Correct Sad Identifications	0.138
	Short Penn Continuous Performance Test: Specificity	0.172	NIH Toolbox Pattern Comparison Processing Speed Test: Age-Adjusted Scale Score	0.127
	Short Penn Continuous Performance Test: True Negatives	0.172	Delay Discounting: Area Under the Curve for Discounting of $40,000	0.126

293

294   **Table 1. Cognitive measures that were highly significantly correlated with CNMs**

13

295

Prediction of life outcomes using CNMs

297 We next investigated whether CNMs could predict life outcomes, complementing

298 conventional behavioral tests (i.e., measures of fluid intelligence).

299 Figs. 3a, 3b and 3c show that predicting with CNMs alone achieved significant predictive

300 value ($P < 10^{-4}$ for income and number of years of education; $P < 2.00 \times 10^{-4}$ for life

301 satisfaction; 10,000 times permutation test). The correlation coefficient (r) was slightly

302 higher than that with fluid intelligence alone for income and life satisfaction, but worse for

303 years of education. Combining both the CNMs and fluid intelligence yielded the highest

304 performance in every case ($P < 10^{-4}$ for all income and years of education; $P < 2.00 \times 10^{-4}$

305 for life satisfaction; 10,000 times permutation test).

306
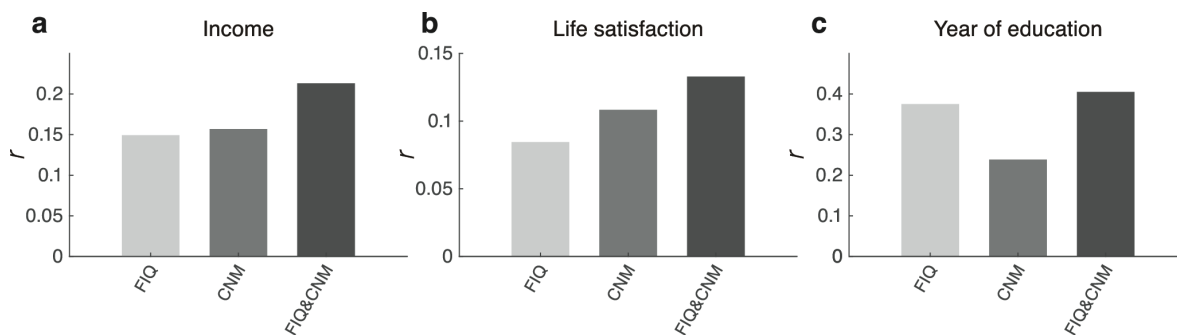
308 **Figure 3. Prediction performance.** Cross validated prediction accuracies by the fluid

309 intelligence obtained by the behavioral test batteries (FIQ; left), the CNMs (middle) and

310 their combination (right) for income, life satisfaction and number of years of education,

311 respectively.

312

Effects of the number of states used for the CNMs

314 We further investigated the effects of the number of states used for identifying the CNMs on

315 the prediction accuracy. Fig. 4a, 4b and 4c show the prediction accuracies using the CNMs

316 with different numbers of states. These figures indicate that the more states we used, the

317 greater accuracy we were able to achieve for predicting life outcomes. We constructed linear

318 regression models, and found that the effects of the number of states were significant for all

14

319   models ($P = 8.15 \times 10^{-13}$ for income; $P = 5.71 \times 10^{-13}$ for life satisfaction; $P = 0.007$ for years

320   of education).

321

322

323   **Figure 4. Relationship between the number of states used for the CNMs and**

324   **prediction performance.** Cross validated prediction accuracies of the CNMs obtained

325   from different numbers of states for income (left), life satisfaction (middle) and number

326   of years of education (right), respectively.

327

328   **Interpretation of the CNMs**

329   To facilitate characterization of the biological substrates of the FCs underlying CNMs, we

330   grouped the 268 ROIs into eight macroscale canonical networks. Figure 5 show the circle

331   plots of the FCs that were correlated with CNM1, CNM2 and CNM3. The numbers of FCs

332   in each of the two macroscale regions (the medial frontal [MF], frontoparietal [FP], default

333   mode network [DMN], subcortical-cerebellum [SC-CB], motor [MTR], visual I [V1], visual

334   II [V2], and visual association [VAssc]) networks are presented as the thickness of the

335   connection lines. Connection lines are colored blue within the same network and red between

336   two networks. Although the FCs were widely distributed rather than locally constrained,

337   there were some differences in the distributions among the CNMs. A certain degree of the

338   FCs in the CNM1 belonged to the networks between cortical and subcortical brain regions,

339   including the medial frontal network. On the other hand, FCs in the CNM2 belonged to the

340   networks within cortical brain regions including the frontoparietal network. Finally, FCs in

341   the CNM3 belonged to both the cortico-cortico and cortico-subcortical networks including

342   both the medial frontal and frontoparietal networks.

343
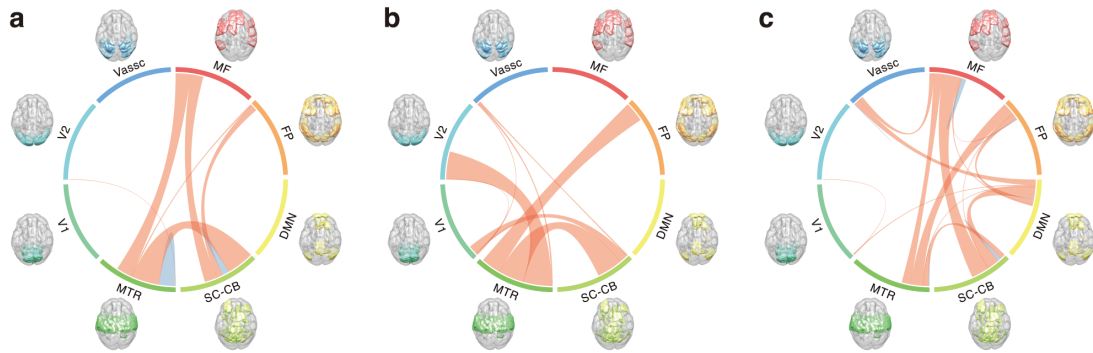
Figure 5. Spatial distribution of the functional connectivity (FC) related to CNMs. The number of FCs between each pair of canonical networks in **(1)** CNM1, **(2)** CNM2 and **(3)** CNM3, respectively. Canonical networks included the medial frontal (MF), frontoparietal (FP), default mode network (DMN), subcortical-cerebellum (SC-CB), motor (MTR), visual I (V1), visual II (V2), and visual association (VAssc). Connection lines are colored blue within the same network and red between two networks.

352 **Discussion**

353

354 In the present study, we conducted, for the first time, a quantitative examination of the

355 potential factors underlying state-unspecific inter-individual variability of whole-brain FC

356 patterns, which we termed CNMs, and investigated their associations with behaviors and life

357 outcomes. Although previous studies have suggested a state-unspecific pattern of FC (Cole

358 et al., 2014; Finn et al., 2015; Tavor et al., 2016), to our knowledge no study has directly

359 defined such FC patterns in a quantitative manner. The CNMs were extracted by M-CCA in

360 a fully cross-validated manner from the fMRI datasets of the HCP, covering a broad range of

361 task and resting states. The CNMs predicted representative intelligence measures including

362 fluid and crystalized intelligence with significant correlations, which could not be achieved

363 without M-CCA (i.e., with PCA alone). We further demonstrated that the CNMs were able to

364 predict several life outcomes, complementing conventional behavioral tests of fluid

365 intelligence. We also found that the more states we used to identify CNMs, the higher

366 accuracy we were able to achieve when predicting life outcomes. The FCs constituting those

367 CNMs were widely distributed throughout the brain rather than being locally constrained.

368

369 Three CNMs were robustly extracted by M-CCA, which correlated significantly with

370 representative intelligence measures (Fig. 2). Intelligence measures are related to a wide

371 range of cognitive functions and predict broad social outcomes such as educational

372 achievement, job performance, health, and longevity (Cattell, 1963; Colom et al., 2010;

373 Gottfredson, 1997). Therefore, the relationships between the CNMs and these measures are

374 intuitive to understand. It is also noteworthy that each CNM correlated with a different

375 dimension of intelligence. That is, CNM1 and CNM3 correlated with fluid intelligence, while

376 the CNM2 correlated with crystalized intelligence. This suggests that these CNMs may have

377 different biological substrates (Fig. 5). Importantly, the CNMs were derived in a fully data-

378 driven, cross-validated manner. The relationship between CNMs and intelligence measures

379 was thus non-trivial. Although our study was inspired by the "positive-negative" neural

380 modes (Smith et al., 2015) which are also correlated with intelligence measures, our CNM

381 analysis fundamentally differs from that used by Smith et al. (2015) in several important

17

382   ways. First, although Smith et al. (2015) obtained their results by optimizing the correlation
383   between behavioral measures and FCs explicitly, our CNM did not use any behavioral
384   measure. Second, while Smith et al. (2015) used resting state data only, our CNM method
385   used multiple states.

386

387   When predicting life outcomes from CNMs alone, CNMs achieved higher prediction
388   accuracies for income and life satisfaction than prediction with conventional intelligence
389   measures alone. In contrast, conventional intelligence measures achieved better prediction
390   for the number of years of education (Fig. 3). These results may reflect different
391   characteristics between biologically defined measures and measures from a behavioral
392   battery. It should be noted that combining the CNMs with fluid intelligence achieved the
393   highest prediction accuracies for all life outcomes. These results indicate that CNMs contain
394   valuable information for predicting behavior that may not be captured by conventional
395   intelligence measures.

396

397   Importantly, using a greater number of states to identify CNMs enabled us to achieve greater
398   prediction accuracy (Fig. 4). This indicates that CNMs were more reliably extracted when
399   considering a greater number of behavioral states. Indeed, the correlation between
400   representative intelligence measures and first principal components derived from each single
401   state were lower than those of the CNMs. Our findings suggest that contrasting many
402   different states, rather than considering any single (typically resting) state, can more reliably
403   identify the neural modes that are able to predict diverse types of individual differences.

404

405   Although all three CNMs were related to the subcortical-networks and motor networks, we
406   observed different trends among them in terms of the related canonical networks (Fig. 5).
407   CNM1, CNM2 and CNM3 were related to the medial frontal network, frontoparietal network,
408   and both networks, respectively. This finding is of interest because CNM1 and CNM2
409   captured different aspects of intelligence (fluid and crystalized intelligence, respectively)
410   while CNM3 was related to both. We also observed that brain regions contributing to all
411   CNMs were widely distributed rather than locally restricted. This is consistent with a

18

412   previous study reporting that brain regions related to intelligence were broadly distributed
413   (Haier et al., 2009). Several previous studies have also reported a relationship between
414   intelligence measures and FCs (Finn et al., 2015; Lerman-Sinkoff et al., 2017; Schultz and
415   Cole, 2016). However, most of these studies have examined only one state.
416

417   Although we focused on state-unspecific neural modes across various states, these modes
418   would be expected to function in a coordinated way with other state-specific neural modes
419   in any particular state. Different neural modes for respective states may have different
420   abilities associated with different neural substrates, which may also cause individual
421   differences in behavior. Thus, it would be useful for future studies to comprehensively
422   compare the relationship between the state-specific and state-unspecific neural modes in
423   terms of their relationship with both cognitive measures and neural substrates.
424

425   In summary, we identified neural modes that appeared to be stable across different states, and
426   quantitatively characterized various individual differences. These components, referred to as
427   CNMs, were identified in a fully data-driven manner using a machine learning technique.
428   The CNMs were significantly correlated with representative intelligence measures as well as
429   life outcomes. Although previous studies suggested the potential of brain networks that are
430   shared among broad states, the current study is the first to quantitatively define such networks
431   and demonstrate that they may have a broad effect on behavior and life outcomes. We believe
432   that the present study provides evidence that state-unspecific brain networks may be related
433   to a diverse range of behaviors and life achievements.
434

442   visualization.

443

References

Barch, D.M., Burgess, G.C., Harms, M.P., Petersen, S.E., Schlaggar, B.L., Corbetta, M., Glasser, M.F., Curtiss, S., Dixit, S., Feldt, C., Nolan, D., Bryant, E., Hartley, T., Footer, O., Bjork, J.M., Poldrack, R., Smith, S., Johansen-Berg, H., Snyder, A.Z., Van Essen, D.C., 2013. Function in the human connectome: Task-fMRI and individual differences in behavior. Neuroimage 80, 169–189. doi:10.1016/j.neuroimage.2013.05.033

Barch, D.M., Yarkoni, T., 2013. Introduction to the special issue on reliability and replication in cognitive and affective neuroscience research. Cogn. Affect. Behav. Neurosci. 13, 687–689. doi:10.3758/s13415-013-0201-7

Cattell, R.B., 1963. Theory of fluid and crystallized intelligence: A critical experiment. J. Educ. Psychol. 54, 1–22. doi:10.1037/h0046743

Cole, M.W., Bassett, D.S., Power, J.D., Braver, T.S., Petersen, S.E., 2014. Intrinsic and task-evoked network architectures of the human brain. Neuron 83, 238–251. doi:10.1016/j.neuron.2014.05.014

Cole, M.W., Ito, T., Bassett, D.S., Schultz, D.H., 2016. Activity flow over resting-state networks shapes cognitive task activations. Nat. Neurosci. 19, 1718–1726. doi:10.1101/055194

Colom, R., Karama, S., Jung, R.E., Haier, R.J., 2010. Human intelligence and brain networks. Dialogues Clin. Neurosci. 12, 489–501.

Dubois, J., Adolphs, R., 2016. Building a Science of Individual Differences from fMRI. Trends Cogn. Sci. 20, 1–19. doi:10.1016/j.tics.2016.03.014

Finn, E.S., Shen, X., Scheinost, D., Rosenberg, M.D., Huang, J., Chun, M.M., Papademetris, X., Todd Constable, R., 2015. Functional connectome fingerprinting: identifying individuals using patterns of brain connectivity. Nat. Neurosci. 18, 1–11. doi:10.1038/nn.4135

Fox, M.D., Greicius, M., 2010. Clinical applications of resting state functional connectivity. Front. Syst. Neurosci. 4, 19. doi:10.3389/fnsys.2010.00019

Geerligs, L., Rubinov, M., Cam-CAN, Henson, R.N., 2015. State and Trait Components of

474   Functional Connectivity: Individual Differences Vary with Mental State. J. Neurosci.

475   35, 13949–13961. doi:10.1523/JNEUROSCI.1324-15.2015

476   Glasser, M.F., Sotiropoulos, S.N., Wilson, J.A., Coalson, T.S., Fischl, B., Andersson, J.L.,

477   Xu, J., Jbabdi, S., Webster, M., Polimeni, J.R., Van Essen, D.C., Jenkinson, M., 2013.

478   The minimal preprocessing pipelines for the Human Connectome Project. Neuroimage

479   80, 105–124. doi:10.1016/j.neuroimage.2013.04.127

480   Gottfredson, L.S., 1997. Why g matters: The complexity of everyday life. Intelligence 24,

481   79–132. doi:10.1016/S0160-2896(97)90014-3

482   Haier, R.J., Colom, R., Schroeder, D.H., Condon, C.A., Tang, C., Eaves, E., Head, K.,

483   2009. Gray matter and intelligence factors: Is there a neuro-g? Intelligence 37, 136–

484   144. doi:10.1016/j.intell.2008.10.011

485   Hotelling, H., 1936. Relations between two sets of variates. Biometrika 28, 321–377.

486   Kettenring, J.R., 1971. Canonical Analysis of Several Sets of Variables. Biometrika 58,

487   433–451.

488   Lerman-Sinkoff, D.B., Sui, J., Rachakonda, S., Kandala, S., Calhoun, V.D., Barch, D.M.,

489   2017. Multimodal neural correlates of cognitive control in the Human Connectome

490   Project. Neuroimage. doi:10.1016/j.neuroimage.2017.08.081

491   Modi, S., Kumar, M., Kumar, P., Khushu, S., 2015. Aberrant functional connectivity of

492   resting state networks associated with trait anxiety. Psychiatry Res. - Neuroimaging

493   234, 25–34. doi:10.1016/j.pscychresns.2015.07.006

494   Power, J.D., Barnes, K. a, Snyder, A.Z., Schlaggar, B.L., Petersen, S.E., 2012. Spurious but

495   systematic correlations in functional connectivity MRI networks arise from subject

496   motion. Neuroimage 59, 2142–54. doi:10.1016/j.neuroimage.2011.10.018

497   Raichle, M.E., 2015. The Brain's Default Mode Network. Annu. Rev. Neurosci. 38, 433–

498   447. doi:10.1146/annurev-neuro-071013-014030

499   Rosenberg, M.D., Finn, E.S., Scheinost, D., Papademetris, X., Shen, X., Constable, R.T.,

500   Chun, M.M., 2016. A neuromarker of sustained attention from whole-brain functional

501   connectivity. Nat. Neurosci. 19, 165–71. doi:10.1038/nn.4179

502   Schultz, D.H., Cole, M.W., 2016. Higher Intelligence Is Associated with Less Task-Related

503   Brain Network Reconfiguration. J. Neurosci. 36, 8551–8561.

504   doi:10.1523/JNEUROSCI.0358-16.2016

505 Smith, S.M., Nichols, T.E., Vidaurre, D., Winkler, A.M., J Behrens, T.E., Glasser, M.F.,
506   Ugurbil, K., Barch, D.M., Van Essen, D.C., Miller, K.L., 2015. A positive-negative
507   mode of population covariation links brain connectivity, demographics and behavior.
508   Nat. Neurosci. 18, 1–7. doi:10.1038/nn.4125

509 Smith, S.M., Vidaurre, D., Beckmann, C.F., Glasser, M.F., Jenkinson, M., Miller, K.L.,
510   Nichols, T.E., Robinson, E.C., Salimi-Khorshidi, G., Woolrich, M.W., Barch, D.M.,
511   Uğurbil, K., Van Essen, D.C., 2013. Functional connectomics from resting-state fMRI.
512   Trends Cogn. Sci. 17, 666–82. doi:10.1016/j.tics.2013.09.016

513 Takagi, Y., Sakai, Y., Abe, Y., Nishida, S., Harrison, B.J., Martínez-Zalacaín, I., Soriano-
514   Mas, C., Narumoto, J., Tanaka, S.C., 2018. A common brain network among state,
515   trait, and pathological anxiety from whole-brain functional connectivity. Neuroimage
516   172, 506–516. doi:10.1016/j.neuroimage.2018.01.080

517 Takagi, Y., Sakai, Y., Lisi, G., Yahata, N., Abe, Y., Nishida, S., Nakamae, T., Morimoto,
518   J., Kawato, M., Narumoto, J., Tanaka, S.C., 2017. A neural marker of obsessive-
519   compulsive disorder from whole-brain functional connectivity. Sci. Rep. 7, 7538.

520 Tavor, I., Parker Jones, O., Mars, R.B., Smith, S.M., Behrens, T.E., Jbabdi, S., 2016. Task-
521   free MRI predicts individual differences in brain activity during task performance.
522   Science 352, 216–20. doi:10.1126/science.aad8127

523 Uğurbil, K., Xu, J., Auerbach, E.J., Moeller, S., Vu, A.T., Duarte-Carvajalino, J.M.,
524   Lenglet, C., Wu, X., Schmitter, S., Van de Moortele, P.F., Strupp, J., Sapiro, G., De
525   Martino, F., Wang, D., Harel, N., Garwood, M., Chen, L., Feinberg, D.A., Smith,
526   S.M., Miller, K.L., Sotiropoulos, S.N., Jbabdi, S., Andersson, J.L.R., Behrens, T.E.J.,
527   Glasser, M.F., Van Essen, D.C., Yacoub, E., 2013. Pushing spatial and temporal
528   resolution for functional and diffusion MRI in the Human Connectome Project.
529   Neuroimage 80, 80–104. doi:10.1016/j.neuroimage.2013.05.012

530 Van Essen, D.C., Ugurbil, K., Auerbach, E., Barch, D., Behrens, T.E.J., Bucholz, R.,
531   Chang, A., Chen, L., Corbetta, M., Curtiss, S.W., Della Penna, S., Feinberg, D.,
532   Glasser, M.F., Harel, N., Heath, A.C., Larson-Prior, L., Marcus, D., Michalareas, G.,
533   Moeller, S., Oostenveld, R., Petersen, S.E., Prior, F., Schlaggar, B.L., Smith, S.M.,

534   Snyder, A.Z., Xu, J., Yacoub, E., 2012. The Human Connectome Project: A data

535   acquisition perspective. Neuroimage 62, 2222–2231.

536   doi:10.1016/j.neuroimage.2012.02.018

537 Via, J., Santamaria, I., Pérez, J., 2005. Canonical correlation analysis (CCA) algorithms for

538   multiple data sets: Application to blind SIMO equalization. Signal Process. Conf. 1,

539   4–7.

540 Vía, J., Santamaría, I., Pérez, J., 2007. A learning algorithm for adaptive canonical

541   correlation analysis of several data sets. Neural Networks 20, 139–152.

542   doi:10.1016/j.neunet.2006.09.011

543